COMPRESSIVE STRENGTH AND STIFFNESS OF GLULAM IN CONTACT WITH MORTAR

Yuichi Kanaya[1], Shun Kosugi[2], Marina Totsuka[3]*, Hiroki Nakashima[4],Masakazu Ikeda [5], Kenji Aoki[6]

ABSTRACT: Recently, applications of timber-concrete composite components have increased in large-scale timber buildings. It is important to understand the compressive behavior of joints between wood and concrete in these components. This study investigates the compressive behavior of glulam in contact with several materials (steel plate, mortar, mortar with epoxy adhesive, and mortar with waterproof paint) and also proposes an effect factor of the materials under compression when in contact with the glulam. Compression tests were conducted on 108 specimens. Our study revealed that when the glulam comes in contact with the mortar, the compressive strength and stiffness decreased because the moisture in the mortar was transferred into the glulam. In addition, inserting an epoxy layer between the mortar and glulam could increase the strength and stiffness due to a prevention of the moisture transfer from the mortar. An evaluation method using the effect factors of the strength is proposed.

KEYWORDS: Glulam, Compression parallel to the grain, Mortar, Timber-concrete composite components, Joint

1 – INTRODUCTION & BACKGROUND

In recent years, constructions of large-scale timber buildings have become increasingly common. Consequently, designers and researchers have developed components that combine various materials, such as concrete and steel, together with timber in some cases to enable the constructions of these buildings.

One example is a timber-concrete composite beam (TCC beam) made of timber beams and a reinforced concrete slab (Fig. 1) [1][2]. During the design process of these components, it is crucial to accurately evaluate behaviour of a contact interface between glulam and concrete, as stress transfer occurs at this interface. However, no evaluation method currently exists that can be used to explain this behaviour.

Furthermore, low-stiffness regions, referred to as damage zones (Fig. 2), are present near butt-ends of a glulam compressed parallel to the grain [3][4]. In the composite components, the damage zone often contacts with various materials [5][6][7]. An effect of the low-stiffness region should also be considered in the design of the TCC. A previous study showed that in specimens with mortar cast directly on the butt-end, both the compressive strength and stiffness parallel to the grain decrease, and the surface strain increases when the compressive stress is applied parallel to the grain [8].
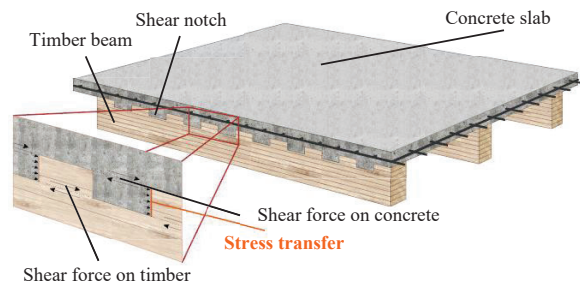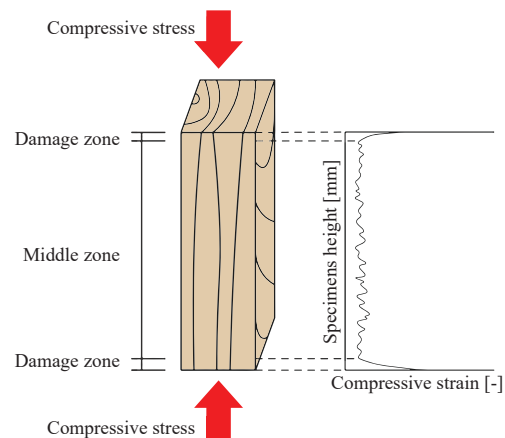

Figure 1: Example of a TCC beam

Figure 2: Overview Diagram of the Damage Zone

---

[1] Yuichi Kanaya, Graduate School of Science and Engineering, Chiba Univ.
[2] Shun Kosugi, Graduate School of Science and Engineering, Chiba Univ.
[3]* Corresponding author, Marina Totsuka, Graduate School of Engineering, Chiba University, Chiba, Japan, ORCID 0000-0001-8548-4996
[4] Hiroki Nakashima, Sumitomo Forestry CO., LTD.
[5] Masakazu Ikeda, Sumitomo Forestry CO., LTD.
[6] Kenji Aoki, Graduate School of Agricultural and Life Sciences, The Univ. of Tokyo

This study aims to clarify the causes of the reduction in the strength and stiffness of the glulam specimens contacted with mortar under the compression parallel to the grain and propose improvement methods. In addition, the influence of the contact materials is quantitatively evaluated for the strength and stiffness.

2 – PROJECT DESCRIPTION

2.1 SUMMARY OF SPECIMENS

Test parameters and an overview of the specimens are shown in Table 1 and Fig. 3. The parameters were shapes of cross-section (75mm×75mm square, φ100 circle in Fig. 4), contact materials (steel plate, mortar 10 mm, mortar 20 mm, epoxy adhesives), and surface treatments (none, waterproof paint layer, epoxy adhesive layer). A height of the glulam of the specimens was $L = 180$ mm. To investigate the effect of a moisture transfer between the mortar and glulam, a waterproof paint layer was inserted as a surface treatment between the glulam and mortar. An epoxy layer was inserted to improve the effect of the damage zone. Fourteen series with a combination of these parameters were prepared, and a total of 84 specimens were tested. The glulam was made of Japanese cedar (*Cryptomeria japonica*) with a grade of E65-F225 according to JAS (Japanese Agricultural Standards). The cutting diagram is shown in Fig. 5. To eliminate the effect of variations in the material properties of glulam, all square-series specimens were created from the same motherboard, and all circle-series specimens were created in the same manner. Specifically, one square sample per series and two circle samples per series were taken from the same motherboard. A total of six rectangular and three cylindrical motherboards without finger joints were prepared, referred to as GL-1 to GL-9.

The mean density of the square specimens is 0.42 g/cm³, with a coefficient of variation of 0.038, and that of circle specimens is 0.43 g/cm³, with a coefficient of variation of 0.056.

The mean moisture content of the square specimens is 14.83 %, with a coefficient variation of 0.050, and that of circle specimens is 13.88 %, with a coefficient variation of 0.017. The moisture content was measured by an oven-dry method according to JIS (Japanese Industrial Standards) A1476 [9].

2.2 SPECIMEN PREPARATION METHOD

The specimens in contact with mortar (75A-2, 100C-2) were fabricated indoors and according to a procedure described below.

1. The waterproof paint or the epoxy adhesive was applied to the butt-end. The specimens were cured in a climate-controlled chamber maintained at 20 ℃ and 65 % relative humidity. The curing duration was at least 24 hours. The epoxy adhesive was applied in two coats.

2. The mortar formwork for the square specimens was made of plywood (Fig. 6), and the circle specimens were made of soft PVC-P desk mats (Fig. 7). Mortar was cast into these moulds, leading to direct contact between the fresh mortar and the butt-end surface of the specimens.
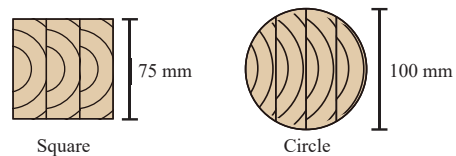

Figure 4: shapes of Cross-Section

Table 1: Test Parameters

Series	75A-1	75A-1-W	75A-2-10	75A-2-10-W	75A-2-10-E	100C-1	100C-2-10
Contact Materials	Steel Plate	Steel Plate	Mortar 10mm	Mortar 10mm	Mortar 10mm	Steel Plate	Mortar 10mm
Surface Treatments	None	Waterproof Paint Layer	None	Waterproof Paint Layer	Epoxy Adhesive Layer	None	None

Series	75A-3	75A-3-W	75A-2-20	75A-2-20-W	75A-2-20-E	100C-2-20	100C-3
Contact Materials	Steel Plate	Epoxy Adhesive	Mortar 20mm	Mortar 20mm	Mortar 20mm	Mortar 20mm	Steel Plate
Surface Treatments	Epoxy Adhesive Layer	Waterproof Paint Layer	None	Waterproof Paint Layer	Epoxy Adhesive Layer	None	Epoxy Adhesive Layer

Square | Circle

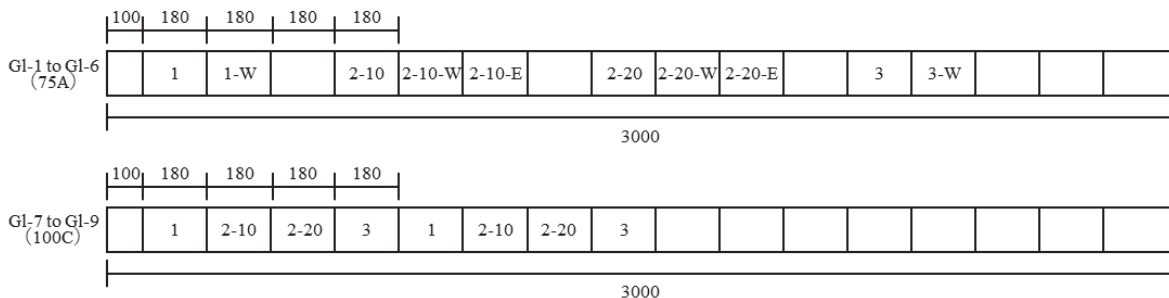*Figure 3: Overview of The Specimens*

Figure 5: Cutting Diagram

342

3. The specimens were cured for more than 28 days in the same climate-controlled chamber.

4. The formwork was then removed before the start of the test, and strain gauges were attached to the specimens.

The specimens with epoxy adhesive on the top surface (75A-3, 100C-3) were prepared by applying a single coat of epoxy resin adhesive, followed by placing a steel plate on the surface to level the interface and then adding a weight on top. Subsequently, the specimens were cured for over 24 hours in the temperature-controlled chamber.

3 – EXPERIMENTAL SETUP

3.1 TEST METHOD

The compression tests were carried out on a universal testing machine with a displacement speed of 0.003 L mm/min according to ASTM D143 [10]. The test setup is shown in Fig. 8. The load was obtained from a load cell. Displacements between the steel plate and 130 mm below the butt-end were obtained using the displacement transducers. The displacement transducers were directly attached to the specimen. Strains at the center of the specimen were recorded by strain gauges on the surface. Furthermore, only 100C-2-20 had strain gauges attached at the center of the mortar. Local strains on the surface of the specimen were obtained using a Digital Image Correlation (DIC) system with a digital camera (Fig. 8).

3.2 DIC SETUP

The measurement range of the surface strains on the surface by the DIC is specified below. The surface strains were applied only to the square specimens. A region excluding the damage zone is referred to as a middle zone (Fig. 1).

(A) Mean value of surface strain in the middle zone

The measurement range was defined as the region excluding 15 mm from the butt-end and 10 mm from both ends, as shown in Fig. 9-A. The strain in the damage zone and the end strain, which is prone to measurement failures, were excluded.

(B) Surface strain distribution in L-direction at 0.4 P_{yield}

On all square specimens, a line was drawn 30 mm downward from the butt-end (red line, Fig. 9-B). On 75A-2-20, a line was drawn 10 mm upward from the butt-end (blue line, Fig. 9-B). The lines were defined as a central 40 mm of the glulam, excluding 17.5 mm from both ends.

(C) Displacement between two points on mortar and glulam surface

Displacements between the wood and mortar were measured on 75A-2. Points at which the displacements were measured were 5 mm upward and 60 mm downward from the butt-end (total 65mm, Fig. 9-C). A total of six displacements were measured for each specimen.

3.3 MORTAR MATERIAL TEST

Mortar samples for material test were a diameter of φ50 mm and a height of 100 mm. A total of 20 cylindrical

samples were prepared. Strain gauges were attached to the central part of both sides of 10 of the total samples. Young's modulus and maximum strength of the samples was calculated with reference to JIS A1149 [11]. A mean value of the maximum strength for all samples was 91.64 N/mm^2, and a mean value of the Young's modulus for the 9 samples was 25.02 kN/mm^2.

4 – RESULTS

4.1 KINKING FAILURE MOOD

Failure characteristics are shown in Fig. 10 and 11. In 75A-2-10, 75A-2-20, 100C-2-10, and 100C-2-20, kink band failure was observed in the damage zone in all specimens. In some specimens, the kink band failure occurred in both the damage zone and the middle zone. In

Figure 6: Moulds for the Square Specimens

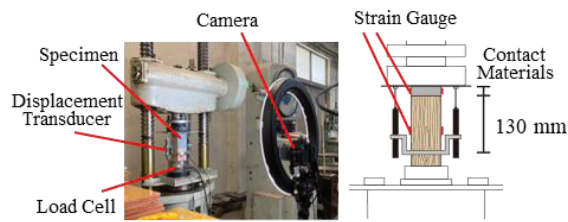*Figure 7: Moulds for the Circle Specimens*
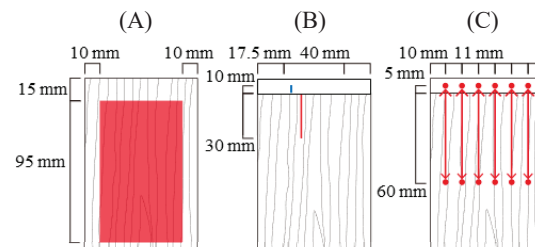

Figure 8: Test Setup

Figure 9: DIC SET UP

Note: Figure (A) is Mean Value of Strain Distribution in the Middle Zone. Figure (B) Surface Strain Distribution in the L-Direction at 0.4Pmax. Figure (C) is Displacement Between Two Points on the Mortar and Glulam Surface.

Figure 10: Damage Zone Failure

Figure 11: Middle Zone Failure

75A-1, 75A-2-10-E, 75A-2-20-E, 75A-3, 100C-1, and 100C-3, the kink band failure occurred only in the middle zone.

4.2 LOAD-DISPLACEMENT RELATIONSHIP

Fig. 12 shows a representative load-displacement relationship of the square specimens. The all specimens depicted in Fig. 12 were made from Gl-1. In all specimens, the load remained constant after reaching the maximum load. Additionally, a yield plateau was observed before reaching the maximum load in 75A-2-10 and 75A-2-20. It is considered that the direct casting of mortar to the butt-end led to a reduction in the yield strength of the glulam-mortar interface. A discoloration of approximately 2 mm in thickness was observed across the entire butt-end in these specimens (Fig. 13). As a result, the discoloration region failed first, followed by the failure of the other zone.

4.3 ASSESSMENT FOR STRENGTH AND STIFFNESS

For each series, mean maximum strength (σ_{max}; calculated using (1)), mean yield strength (σ_{yield}; calculated using (2)), and two mean stiffness calculated using displacement transducers (E_W) and using DIC (E_{W_DIC})) were calculated from the test results (see Tables 2 and 3).

$$\sigma_{max} = \frac{P_{max}}{A} \tag{1}$$

$$\sigma_{yield} = \frac{P_{yield}}{A} \tag{2}$$

Where σ_{max} = maximum strength ($\times 10^3$ N/mm^2), P_{max} = maximum load (kN), A = cross-sectional area (mm^2), σ_{yield} = yield strength ($\times 10^3$ N/mm^2), and P_{yield} = yield load (kN).

The mean yield strength (σ_{yield}) was calculated only for 75A-2-10, 75A-2-20, 100C-2-10, and 100C-2-20.

The E_W and E_{W_DIC} are the stiffness, including the damage zone. The deformation of the mortar part was excluded, and the stiffness corresponds to that of the glulam only. To eliminate an initial slip, the E_W and E_{W_DIC} were calculated using (3), (4), (5), (6), and (7) within the range of 0.25 to 0.4 P_{max} or 0.4 P_{yield}.

$$E_W = \frac{0.4\,P_{max} - 0.25\,P_{max}}{\delta'_{0.4\,P_{max}} - \delta'_{0.25\,P_{max}}} \cdot \frac{L}{A} \tag{3}$$

$$\delta'_t = \delta_t - \frac{P_t \cdot L}{E_M \cdot A} \tag{4}$$

$$E_{W\_DIC} = \frac{0.4\,P_{max} - 0.25\,P_{max}}{\delta''_{0.4\,P_{max}} - \delta''_{0.25\,P_{max}}} \cdot \frac{L'}{A} \tag{5}$$

$$\delta''_t = \delta_{t\_DIC} - \frac{P_t \cdot L}{E_M \cdot A} \tag{6}$$

$$E_M = \frac{1/3\,P_{max} - P_{50}}{(\varepsilon''_{1/3\,P_{max}} - 50) \cdot A} \tag{7}$$

Where E_W = stiffness calculated using displacement transducers (kN/mm^2), L = displacement measurement
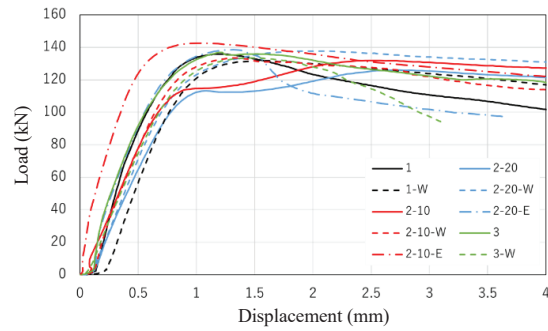

Figure 12: Load-Displacement Relationship of Gl-1

Figure 13: Discoloration of Butt-End

Table 2: Maximum Strength and Yield Strength

Series	mm²)		mm²)	
	Mean	CV	Mean	CV
75A-1	26.11	0.081		
75A-1-W	25.60	0.100		
75A-2-10	25.57	0.055	22.85	0.074
75A-2-10-W	25.73	0.056		
75A-2-10-E	26.49	0.052		
75A-2-20	24.84	0.065	22.63	0.076
75A-2-20-W	25.61	0.069		
75A-2-20-E	26.52	0.063		
75A-3	27.14	0.065		
75A-3-W	26.27	0.062		
100C-1	32.60	0.052		
100C-2-10	30.35	0.062	26.91	0.064
100C-2-20	29.33	0.068	25.24	0.084
100C-3	32.53	0.042		

Table 3: Stiffness

Series	E_W mm²)		E_{W_DIC} mm²)	
	Mean	CV	Mean	CV
75A-1	6.27	0.099		
75A-1-W	5.94	0.293		
75A-2-10	5.98	0.239	3.32	0.079
75A-2-10-W	6.41	0.159	5.39	0.366
75A-2-10-E	8.84	0.149	6.80	0.190
75A-2-20	5.27	0.285	4.63	0.382
75A-2-20-W	6.27	0.108	6.93	0.285
75A-2-20-E	9.38	0.282	6.68	0.179
75A-3	5.67	0.218		
75A-3-W	5.71	0.260		
100C-1	8.38	0.113		
100C-2-10	6.21	0.200		
100C-2-20	4.32	0.189		
100C-3	7.42	0.164		

length = 130 mm, δ_t = displacement measured by the displacement transducers at time t (mm), P_t = load at time t (kN), E_M = stiffness of mortar part in the 75A-2-10, 75A-2-20, 100C-2-10, and 100C-2-20 (kN/mm²), E_{W_DIC} = stiffness calculated using DIC in Section 3.2(C) (kN/mm²), L' = displacement measurement interval between two points (mm), δ_{t_DIC} = displacement between two points on mortar and glulam surface by DIC at time t, ε'' = strain measured by strain gauges attached at the center of the mortar of 100C-2-20 or Mortar samples for a material test ($\times 10^6$), and P_{50} = load at $\varepsilon'' = 50 \times 10^6$ (kN).

Stiffness of mortar part (E_M) for the no surface treatment specimens was taken as the mean values obtained from 100C-2-20. The mean value was calculated based on the strain gauges attached to both sides of the mortar part of 100C-2-20 (Fig. 7). For the specimens with a waterproof paint layer or an epoxy adhesive layer, the mean values obtained from the mortar material test were used.

The stiffness of the middle zone for each series, calculated from the strain gauge values (E_{mid}), and that calculated using DIC in Section 3.2(A) (E_{mid_DIC}), are shown in Table 4. E_{mid} and E_{mid_DIC} were calculated using (8) and (9).

$$E_{mid} = \frac{0.4\,P_{max} - 0.25\,P_{max}}{(\varepsilon_{0.4\,P_{max}} - \varepsilon_{0.25\,P_{max}}) \cdot A} \quad (8)$$

$$E_{mid\_DIC} = \frac{0.4\,P_{max} - 0.25\,P_{max}}{(\varepsilon'_{0.4\,P_{max}} - \varepsilon'_{0.25\,P_{max}}) \cdot A} \quad (9)$$

Where E_{mid} = stiffness of the middle zone calculated using displacement transducers (kN/mm²), E_{mid_DIC} = stiffness of the middle zone calculated using DIC (kN/mm²), ε = strain measured by strain gauges ($\times 10^6$), and ε' = mean value of surface strain in the middle zone measured by DIC ($\times 10^6$).

5 – DISCUSSION

5.1 PROPERTIES OF MORTAR PART IN SPECIMENS

After the test, the specimens in contact with mortar (75A-2-10, 75A-2-10-W, and 75A-2-10-E) were decomposed into the glulam and mortar parts. The contact interface in the mortar part is shown in Fig. 14. In 75A-2-10, an unevenness of annual rings of the timber was transferred onto the mortar part. The unevenness was smaller in 75A-2-10-W than in 75A-2-10. The contact interface was almost flat in 75A-2-10-E. Furthermore, the mortar and timber peeled off in some specimens during demoulding in 75A-2-10 but not in 75A-2-10-W and 75A-2-10-E. This indicates that the specimens in direct contact between the glulam and mortar parts are likely to have smaller adhesion forces.

The stiffnesses of the mortar in 100C-2-20 and the Young's modulus of the samples of the material test are shown in Fig. 15. The stiffnesses and the Young's modulus were calculated (8). The stiffness of the

specimens decreased by approximately 10% compared to the Young's modulus of the material test.

Fig. 16 shows the strain distributions on the surface of the mortar part in the specimens at 0.4 P_{max}. The measurement region is shown in Section 3.2 (B). The maximum strains in the waterproof layer specimens (dashed line in Fig. 16) were much smaller than those in the specimens in direct contact with the mortar (solid line in Fig. 16).

Table 4: Stiffness of Middle Zone

Series	E (mm²)		E_{d_DIC} (mm²)	
	Mean	CV	Mean	CV
75A-1	5.40	0.064	5.34	0.210
75A-1-W	5.62	0.153	5.52	0.373
75A-2-10	8.27	0.342	7.46	0.635
75A-2-10-W	4.62	0.076	6.79	0.319
75A-2-10-E	5.54	0.056	6.45	0.231
75A-2-20	4.43	0.144	7.33	0.288
75A-2-20-W	5.43	0.168	6.81	0.282
75A-2-20-E	5.06	0.041	6.29	0.176
75A-3	4.30	0.135	8.39	0.226
75A-3-W	5.51	0.108	6.53	0.404
100C-1	10.31	0.160		
100C-2-10	9.91	0.201		
100C-2-20	9.97	0.066		
100C-3	10.47	0.256		

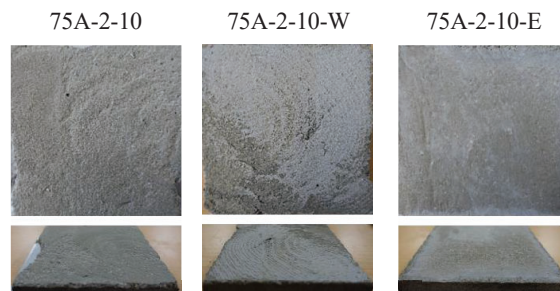75A-2-10   75A-2-10-W   75A-2-10-E

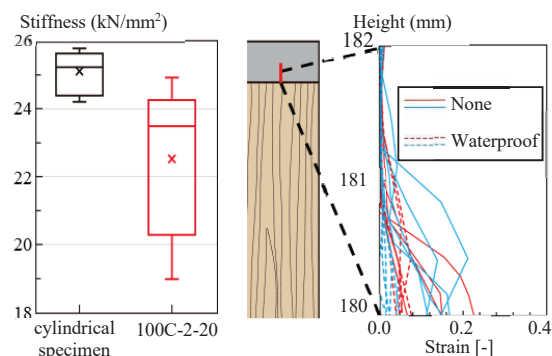

Figure 14: Surface of Mortar

Figure 15: Surface of Mortar   *Figure 16: Mortar Surface Strain Distributions*

5. 2 RELIABILITIES OF THE E_W VALUES

Comparison between the E_W (calculated by using displacement transducers) and E_{mid} (calculated by using the strain gauges) for 75A-1 is shown in Table 5. Gl-1 represents the motherboard, meaning that E_W and E_{mid} of Gl-1 are each calculated for the same specimen. The stiffness of the damage zone was lower than that of the middle zone. E_W included both the middle zone and the damage zone, whereas E_{mid} included only the middle zone. Therefore, the expected relationship was $E_W < E_{mid}$. However, E_W was found to be higher than E_{mid}.

The load-strain relationship of E_{mid} and E_{W_DIC} for 75A-1 is shown in Fig. 17. The same color line represents the specimen prepared from the same glulam. While differences were observed in the initial slip, the slopes around 0.4 P_{max} were generally consistent.

The load-strain relationship of the E_{mid} and E_{mid_comp} for the specimen prepared from the same motherboard is shown in Fig. 18. The E_{mid_comp} was calculated from the values of displacement transducers mounted on a compress meter (Fig. 19). E_{mid_comp} was calculated using (10).

$$E_{mid\_comp} = \frac{0.4\,P_{max} - 0.25\,P_{max}}{\delta'''_{0.4\,P_{max}} - \delta'''_{0.25\,P_{max}}} \cdot \frac{L'}{A} \quad (10)$$

Where E_{mid_comp} = stiffness of the middle zone calculated using a compress meter (kN/mm²), δ'''_t = relative displacement of the fixed ring at time t (mm), and L' = distance between fixed rings (mm)

The E_{mid} and E_{mid_comp} showed general consistency. This indicates that there may have been an issue with the measurement method in which displacement transducers which were directly attached to the specimen.

Comparisons of the surface treatments at 75A-2-10 for E_W and E_{W_DIC} are shown in Table 6. The order relationships between epoxy, waterproof, and no surface treatments were generally consistent between E_W and E_{W_DIC} for each motherboard.

Therefore, although the actual values of E_W are unreliable, the order relationship between epoxy, waterproof, and no surface treatments of the E_W can be considered reliable. From this point onward, the E_W will focus solely on comparisons in this paper.

5. 3 COMPARISONS OF THE CONTACT MATERIALS

The maximum strength (σ_{max}) and the stiffness (E_W) for each series are shown in Fig. 20 and 21, respectively. The horizontal axis represents the contact materials, the marker color indicates the surface treatments and the marker shape indicates the cross-section.

For the σ_{max}, compared to 75A-1, 75A-2-10 and 75A-2-20 were approximately 13% lower, while 75A-3 was slightly higher. For the E_W, 75A-1 was highest, followed by 75A-2-10 and 75A-3, which were comparable, while 75A-2-20 was the lowest. In contrast, for both the σ_{max}

and E_W in the circle specimens, 100C-1 exhibited the highest value, followed by 100C-3, 100C-2-10, and 100C-2-20 in that order.

In the no-surface treatment specimens, the surface strain distribution in the L-direction at 0.4 P_{max} is shown in Fig. 22. The calculation method is in Section 3.2 (B). The strain in the damage zone was greatest for 75A-2-10 and 75A-2-20 (which exhibited similar values), followed by 75A-1 and 75A-3. This trend did not correspond to the order of the E_W. The trend of increased susceptibility to deformation due to the direct casting of mortar to the butt-end was the same as the E_W. However, the trend of inserting the epoxy adhesive layer was different as the E_W.

Table 5: Comparison of E_W and E_{mid} of 75A-1

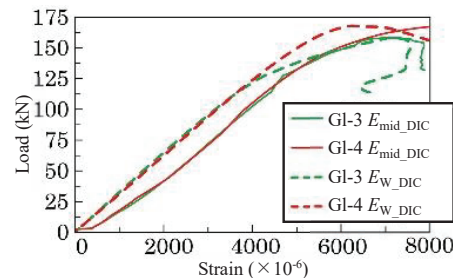| 75A-1	Base Glulam						Mean	CV
	Gl-1	Gl-2	Gl-3	Gl-4	Gl-5	Gl-6		
E_W	6.44	5.68	6.23	7.47	5.58	6.23	6.27	0.10
E		4.93	5.74	5.53			5.40	0.06

Figure 17: Load- strain Relationship of E_{mid} and E_{W_DIC}
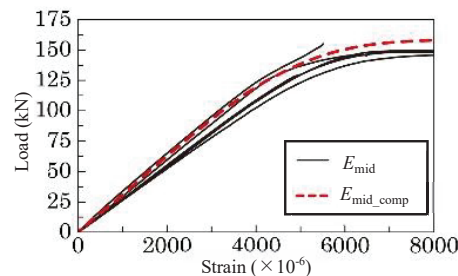

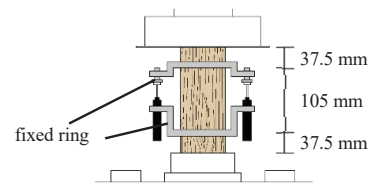Figure 18: Load- strain Relationship of E_W and E_{mid_DIC}

Figure 19: Mounting Position of Compress meter

Table 6: Comparison of Surface Treatments E_W and E_{W_DIC}

Base Glulam	Order Relation							
	E_W				E_{W_DIC}			
Gl-1	Epoxy	>	Waterproof	>	None	Epoxy	>	Waterproof	>	None
Gl-2	Epoxy	>	Waterproof	>		Epoxy	>	Waterproof	>	
Gl-3	Epoxy	>	None	>	Waterproof	Waterproof	>		>	
Gl-4	Waterproof	>	Epoxy	>	None	Waterproof	>	Epoxy	>	None
Gl-5	Epoxy	>	Waterproof	>	None	Epoxy	>	Waterproof	>	None
Gl-6	Epoxy	>	Waterproof	>	None	Epoxy	>	Waterproof	>	None
Mean	Epoxy	>	Waterproof	>	None	Epoxy	>	Waterproof	>	None

346

5. 4 EFFECTS OF MORTAR MOISTURE TRANSFER

By comparing the no-surface treatment specimens (black in Fig. 20 and 21) and the waterproof specimens (red in Fig. 20 and 21), the effect of the moisture transferred from the mortar to glulam was assessed. The σ_{max} and E_W ware compared. For both the σ_{max} and E_W, compared to 75A-2-10, both 75A-2-10-W and 75A-1 exhibited higher values. This trend was also observed for 75A-2-20-W (thicker mortar layer). These results indicate that the effect of the moisture transfer from the mortar to the glulam led to the reduction in the σ_{max} and E_W, irrespective of the mortar thickness.

In waterproof paint layer treatment specimens, the surface strain distribution in the L-direction at 0.4 P_{max} is shown in Fig. 23. Comparing the surface strain distribution to 75A-2-10 (red line in Fig. 23), the strain in the damage zone decreased in 75A-2-10-W (red dashed line in Fig. 23). Furthermore, comparing the waterproof specimens, similar strain distributions were observed for all contact materials. These trends are consistent with the comparison of the E_W. These results indicate that the moisture transfer also affected the increase in strain in the damage zone.

5. 5 REINFORCEMENT EFFECT OF EPOXY ADHESIVES

In the previous study [8], a slight increase in the maximum strength and an improvement in the stiffness were reported for specimens inserted with the epoxy layer between the glulam and steel plate. In the present study,

inserting the epoxy layer between the glulam and mortar is proposed as a solution for reducing the σ_{max} and E_W in the mortar specimens.

For the σ_{max}, compared to 75A-2-10, 75A-2-10-E was higher and 75A-1 was slightly higher. This trend was also observed for 75A-2-20-E (thicker mortar layer). This indicates that the decrease in the maximum strength caused by the mortar casting was counteracted. Furthermore, for the E_W, compared to 75A-1, 75A-2-10-E and 75A-2-20-E were significantly higher.

In the epoxy adhesive layer treatment specimens, the surface strain distribution in the L-direction at 0.4 P_{max} is shown in Fig. 24. Compared to 75A-2-10 (red line in Fig. 24), the strain in the damage zone of 75A-2-10-E significantly decreased and was almost zero (red chain line in Fig. 24). This indicates that inserting the epoxy adhesive layer can reinforce the damage zone.

5. 5 QUANTITATIVE EVALUATION

In this experiment and the FY2022 experiment [8] (96 specimens), the effects of the contact materials and surface treatments are evaluated using the rate of change α. The α was calculated using (11)

$$\alpha = \frac{1}{n}\sum_{k=1}^{n} \frac{\text{m,Gl}-k}{\text{0,Gl}-k} \qquad (11)$$

Where n = number of the motherboard, $\sigma_{m,Gl-k}$ = The maximum strength or yield strength of series m and the motherboard number k [N/mm^2], and $\sigma_{0,Gl-k}$ = The
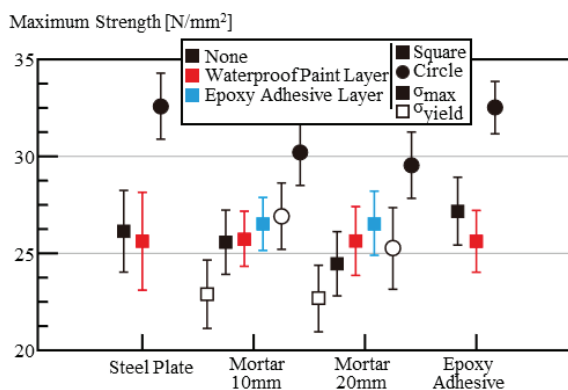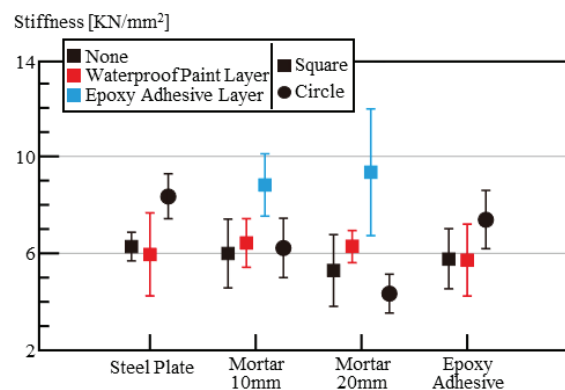

Figure 20: Maximum Strength
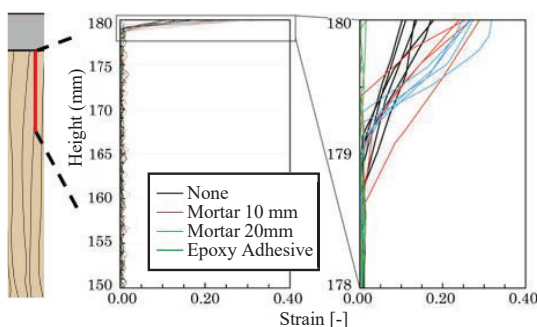

Figure 21: Stiffness

Figure 22: Surface Strain Distributions 75A-1, 75A-2-10, 75A-2-20 and 75A-3
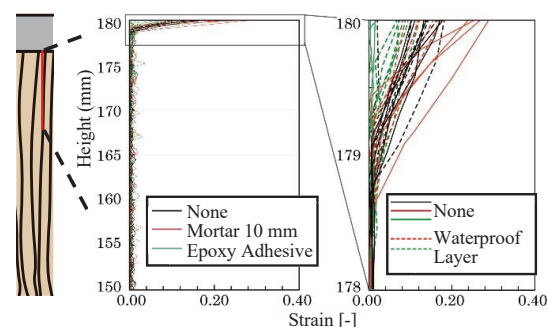

Figure 23: Surface Strain Distributions 75A-1, 75A-2-W, 75A-2-10, 75A-2-10-W, 75A-3, and 75A-3-W

347

maximum stress of specimen (steel plate, no surface treatments) with the motherboard number k [N/mm²].

The specimens (steel plate, no surface treatments) are defined as the benchmark. At the maximum strength ($\sigma_{\max}$) for each specimen, the rate of change was calculated using the benchmark prepared from the same motherboard, and the mean value was taken as α. The same calculation method was applied to determine α for the stiffness as follows.

$$\alpha = \frac{1}{n}\sum_{k=1}^{n} \frac{E_{Wm,Gl-}}{E_{W0,Gl-}} \qquad (12)$$

Where n = number of the motherboard, $E_{Wm,Gl-k}$ = The stiffness of series m and the motherboard number k [kN/mm²], $E_{W0,Gl-k}$ = The stiffness of specimen (steel plate, no surface treatments) with the motherboard number k [kN/mm²]

The α is set with a reference value of 1.0, quantitatively showing the effect of each series.

The rate of change, α, for the $\sigma_{\max}$ is shown in Fig. 25. The horizontal axis represents the contact materials, the marker color represents the surface treatments, and the marker shape represents the experimental year. In the specimens casting mortar directly on the butt-end, the α decreased and became approximately 0.75~0.80. Furthermore, regardless of the mortar casting, for the specimens inserting the waterproof paint layer or the epoxy adhesive layer, α became approximately 1.0. This trend indicates that the insertion of the epoxy layer or the waterproof paint layer between the mortar and butt-end can partially prevent the reduction of $\sigma_{\max}$.

The rate of change, α, for the stiffness (E_{W}) is shown in Fig. 26. In the specimens casting mortar directly on the butt-end, the α decreased in the same way as the $\sigma_{\max}$. By inserting the waterproof layer between the mortar and butt-end (red in Fig. 26), the α became approximately 1.0. Furthermore, by inserting the epoxy adhesive layer between the mortar and butt-end (blue in Fig. 26), the α became very large. From these trends, in the case of E_{W}, the waterproof paint appears effective in preventing the reduction caused by the damage zone, while the epoxy adhesive appears effective in reinforcing the damage zone.

6 – CONCLUSION

The compression tests parallel to the grains were conducted on 84 specimens to investigate the compressive behavior of the glulam in contact with several materials (steel plate, mortar, mortar with epoxy adhesive, and mortar with waterproof paint) near the butt-end. Based on the test results, the following conclusions were drawn.

For the glulam specimens in contact with the mortar, the compression strength and stiffness decreased compared to the specimens without mortar. The kink band failure occurred at only the damage zone and the load yielded. For the mortar part, the young's modulus was lower than that of the material tests and the surface strain near the glulam was bigger. For the glulam part, the stiffness decreased, and surface strain near the butt-end of the glulam increased. This is because the interface properties of the mortar and glulam changed, casting mortar directly on the butt-end of the glulam. These results indicate that defects occurred in the mortar and glulam parts near the joint between the mortar and the glulam.

For the specimens inserting the waterproof layer between the mortar and butt-end, the compression strength, stiffness, and surface strain of the glulam part were comparable to those of the specimens without mortar. It is because, by inserting the waterproof layer between the mortar and butt-end, the mortar moisture movement from the mortar to the glulam was constrained. Therefore, the mortar moisture movement may negatively affect its material properties.
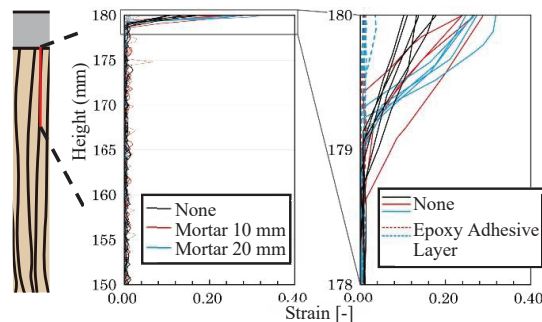

Figure 24: Surface Strain Distributions
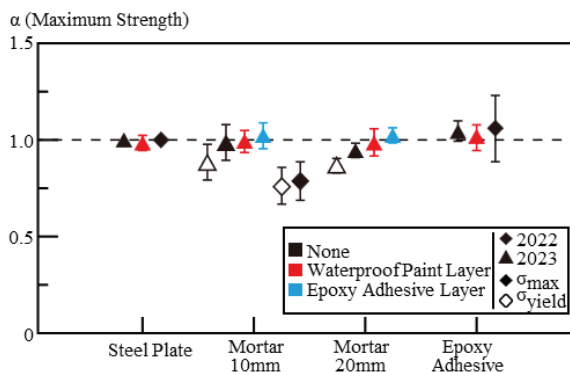*75A-1, 75A-2-10, 75A-2-20 and 75A-3*
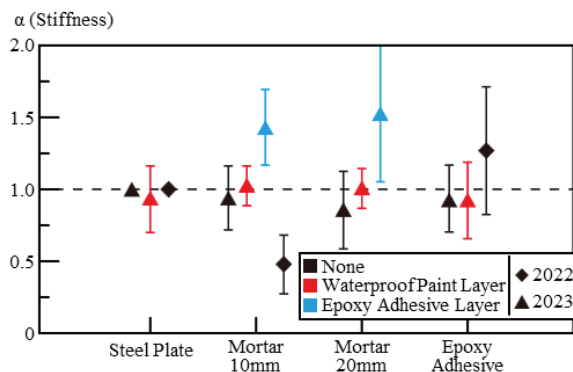

Figure 25: α (Maximum Strength)

Figure 26: α (Stiffness)

For the specimens inserting the epoxy adhesive layer between the mortar and butt-end, the stiffness increased, and the surface strain of the glulam part was smaller compared to the specimens without mortar. The kink band failure occurred at only the middle zone. These results indicate that inserting the epoxy adhesive layer is effective as reinforcement for the damage zone.

The evaluation using the rate of change α indicated that by casting mortar directly on the butt-end, the maximum strength decreases to approximately $\alpha = 0.75$. In addition, stiffness was found to be $\alpha < 1$.

The results of this study suggest that the reduction in both strength and stiffness may occur in TCC beam with direct contact between glulam and concrete. Future work will focus on conducting shear tests using specimens that replicate the shear connectors of the beam to investigate the effect of concrete on the strength and stiffness of glulam.

7 – REFERENCES

Citations: References are given in square brackets like this [1]. Examples:

[1] A. Dias, J. Schänzlin, P. Dietsch, "Design of timber-concrete composite structures." A State-of-the-Art Report by COST Action FP1402/WG (2018), Shaker Verlag. Germany Herzogenrath.

[2] A. Dias, J. Skinner, K. Crews, T. Tannert, "Timber-concrete-composites increasing the use of timber in construction." European Journal of Wood and Wood Products (2015), pp. 1-9

[3] J. Xavier, A. de Jesus, J. Morais, J. Pinto, "Stereovision measurements on evaluating the modulus of elasticity of wood by compression tests parallel to the grain", Construction and Building Materials 26 (2012), pp. 207-215

[4] M. Totsuka, R Jockwer, K Aoki, M Inayama. "Experimental study on partial compression parallel to grain of solid timber", Journal of Wood Science 67 (2021), Article number: 39

[5] D. Yeoh, M. Fragiacomo, B. Deam, "Experimental behaviour of LVL–concrete composite floor beams at strength limit state." Engineering Structures 33 (9) (2011), pp. 2697-2707

[6] A. Dias, U. Kuhlmann, K. Kudla, S. Mönch S, A. M. A. Dias, "Performance of dowel-type fasteners and notches for hybrid timber structures." Engineering Structures vol. 171(2018), pp. 40-46

[7] A. Dias, U. Kuhlmann, K. Kudla, S. Mönch S, A. M. A. Dias, "Structural performance, and failure mechanism, of hardwood cross laminated timber concrete composite under shear load." World Conference on Timber Engineering (2023), pp. 41-50

[8] S. Kosugi, M. Totsuka, H. Nakashima, M. Ikeda, K. Aoki, "Compressive behavior of wood contact with mortar and epoxy resin adhesives." European journal of wood and wood products, in press

[9] JIS A 1476 (2016), "Method for Determination of Moisture Content in Building Materials."

[10] ASTM, "Standard Test Methods for Small Clear Specimens of Timber." D143-14

[11] JIS A1149 (2017), "Method of test for static modulus of elasticity of concrete. Japanese 507 Industrial Standards."